

Dynamic Pilot Design for Multicast in the Internet of Vehicles Running at Different Speeds

Yuli Yang, *Senior Member, IEEE*, and Bingli Jiao, *Senior Member, IEEE*

Abstract—High mobility of vehicles causes time-frequency selective fading over physical channels within the Internet of vehicles (IoV). To improve the resource utilisation efficiency, a novel transmission strategy, based on dynamic pilot design, is proposed in this paper to reduce the pilot consumption in doubly selective channel estimation for the multicast to vehicles running at different speeds. As the channel coherence time is mainly influenced by the receiver mobility in the multicast from a base station to vehicles, we define a multicast block as the channel coherence time of the slowest vehicle in the multicast group, where common pilot symbols are shared. Then, the multicast data destined for different vehicles are loaded into the block according to their own channel coherence times. To evaluate the performance and resource utilisation of our dynamic pilot design, the metrics of overhead rate, spectral efficiency, and energy efficiency are formulated for the IoV multicast using multiple-input-multiple-output (MIMO) orthogonal frequency division multiplexing (OFDM) transmissions. In terms of these three metrics, illustrative numerical results on the comparisons between our dynamic pilot design and the conventional counterpart are provided, which not only substantiate that the former outperforms the latter but also present useful tools and specifications for the pilot design in the IoV multicast using MIMO-OFDM transmissions over doubly selective channels.

Index Terms—Internet of vehicles (IoV), doubly selective channel estimation, dynamic pilot design, overhead rate, spectral efficiency, energy efficiency.

I. INTRODUCTION

The Internet of vehicles (IoV) has been significantly developed by powerful wireless communication and computation technologies, which will provide integrated services in support of smart transport and smart city, through the information exchange between public networks and vehicles [1], [2]. Concerning the physical-layer design, the major challenge faced by the IoV is the time-frequency selective fading caused by the high mobility of vehicles, which results in the resource utilisation efficiency loss as pilot symbols are continually needed in the fast-varying channel estimation [3], [4].

To achieve high resource utilisation efficiency while improving the channel estimation performance, how to distribute pilot symbols and allocate their transmit power have been investigated, see [5]–[18] and the references therein. In the literature, the optimal pilot design has been obtained for point-to-point vehicular communications, which can be readily applied into multicast services with uniform-speed vehicles. However, the vehicles usually run at different speeds in practical IoV

multicast services, where the optimal pilot design needs to be addressed, specifically for ultra-reliable and low-latency communications [19], [20]. Against this backdrop, we intend to further improve the resource utilisation efficiency through dynamic pilot design, which will optimise the deployment of common pilot symbols in the multicast from a base station to vehicles running at different speeds.

A. Related Works

For improving the performance of wireless communications over fading channels, pilot symbol assisted modulation (PSAM) is a commonly used technique, where known pilot symbols are inserted periodically within the unknown data. In this way, authentic channel state information (CSI) can be obtained for coherent signal detection at minimum computational complexity [5].

The placement of pilot symbols and their power allocation play a vital role in the channel estimation [6], [7]. In [8], the pilot design was optimised for maximising the achievable data rate of block transmissions over time-frequency selective fading channels. Moreover, recurrent channel estimation methods [9]–[11] have been proposed based on the optimal design of segmented data rates. In [12], the design of pilot symbols was analysed for orthogonal frequency division multiplexing (OFDM) systems over doubly-selective channels. In [13], the pilot design for OFDM systems was optimised in the case of imperfect channel state prediction. In [14], a pilot contamination elimination scheme was introduced for multi-antenna aided OFDM systems to reduce the training duration.

Specifically for the high-mobility environment, an iterative channel estimation approach was developed in [15] using equispaced pilot symbols for an OFDM system of multiple-input-multiple-output (MIMO) configuration. Then, a reduced-complexity maximum *a posteriori* probability channel estimator with iterative data detection was introduced in [16] for mobile MIMO-OFDM systems. In [17], an information-guided pilot design was proposed to improve the spectral efficiency of OFDM-based vehicular communications. In [18], a pilot design optimisation method was proposed based on the Markov decision process for vehicle-to-everything (V2X) communications to support the IoV applications.

A main challenge faced by V2X communications is the time-frequency selective fading over physical channels, caused by the high mobility of vehicles. In [21], both time and frequency division multiplexed pilots have been considered in massive MIMO-OFDM systems. In [22], the doubly selective channel estimation was analysed in large-scale MIMO systems, where a pilot pattern was introduced by inserting guard

Yuli Yang is with the School of Engineering, University of Lincoln, Lincoln LN6 7TS, U.K. (e-mail: yyang@lincoln.ac.uk).

Bingli Jiao is with the Department of Electronics, Peking University, Beijing 100871, China (e-mail: jiaobl@pku.edu.cn).

TABLE I
CONTRASTING THE NOVELTY OF OUR WORK TO THE LITERATURE

Contributions	This Work	[5]	[6], [7]	[8]–[14]	[17], [18]	[15], [16], [21]–[23]	[24]	[32]	[33]–[35]
Channel Estimation	✓	✓	✓	✓	✓	✓	✓		
Doubly Selective Channels	✓			✓	✓	✓	✓		
MIMO Configuration	✓		✓			✓		✓	
Point-to-Point Communications	✓	✓	✓	✓	✓	✓	✓		
High-Mobility Environment	✓				✓	✓	✓		
Multicast Services	✓							✓	✓
Different Speeds in IoV	✓						✓		

pilots to deal with the inter carrier interference. In [23], a data-aided doubly selective channel estimation scheme was proposed, where the affine-precoded superimposed pilot design was exploited for millimetre wave MIMO-OFDM Systems. In [24], orthogonal time-frequency space modulation is applied to the IoV, where the embedded pilot design was discussed for a vehicle moving at a low speed, a high speed, and a very high speed.

B. Motivation and Novelty

The IoV, established for connecting vehicles and roadside infrastructures, is facing many challenges owing to the high mobility of vehicles. One of them is the doubly selective channel estimation, which requires a high volume of pilot overhead for estimating a large number of channel coefficients, specifically in large-scale MIMO systems. On the other hand, mobile data traffic is anticipated to reach 288EB per month in 2027 [25], which not only requires service providers to reduce energy consumption for lower carbon emissions but also inspires them to improve spectral efficiency for higher effective throughput. From service providers' perspective, the key to increased profitability of their businesses is providing high-volume data services with better quality of service (QoS) and higher network capacity, in an energy-efficient and spectrum-efficient manner, since higher resource utilisation efficiency directly contributes to the cost reduction in the consumption of energy and spectrum resources.

The services in the IoV can be classified into three types: broadcast, unicast, and multicast. The term *broadcast* refers to the service in which the base station transmits a common message to multiple vehicles. The term *unicast* refers to the service in which the base station transmits an individual message to each vehicle. The term *multicast* refers to the service in which the base station transmits multiple messages simultaneously through a single packet and each message is addressed to a single vehicle or certain vehicles [26].

As an efficient approach for boosting the resource utilisation efficiency, the multicast has been exploited in a wide range of applications [27]–[31]. Using a common packet to accommodate multiple messages destined for multiple vehicles, the multicast services in the IoV will reduce the energy consumption and improve the spectral efficiency while guaranteeing the QoS [32]–[34]. In particular, the transparent multicast transport enables the 5G network to provide a cost-effective delivery mode for multimedia [35]. However, since there are

multiple vehicles in the multicast group and the vehicles are likely to run at different speeds, the pilot overhead will have to consume abundant resources.

Motivated by the aforementioned issues, we propose a novel pilot design for the IoV multicast to multiple vehicles running at different speeds, where common pilot symbols are shared in the multicast group and dynamic design is determined by various speeds of the vehicles, to significantly reduce the pilot overhead required in the doubly selective channel estimation. Specifically, the novelty of our work is compared with related works of channel estimation and pilot design in Table I at a glance.

C. Contributions

The attractive features offered by our dynamic pilot design are summarised below.

1) *Pilot Overhead Reduction*: Different from the conventional design of pilot patterns determined by a point-to-point link, we consider the dynamic pilot design in multicast services. Since common pilot symbols are shared among multiple vehicles, the pilot overhead is dramatically reduced.

2) *Multicast to Vehicles Running at Different Speeds*: The pilot design, conceived in previous works, for point-to-point vehicular communications can be utilised in the multicast to uniform-speed vehicles. In this work, our dynamic pilot design is optimised for the multicast to vehicles running at different speeds.

3) *Resource Utilisation Efficiency Improvement*: As the pilot overhead is reduced in our dynamic pilot design, the spectral efficiency will be improved due to higher data rate, and the energy efficiency will be improved due to higher throughput at a given power consumption.

The main contribution of this article are highlighted by the following three aspects.

1) *Principle*: To improve the resource utilisation efficiency in the IoV, dynamic pilot design for doubly selective channel estimation is conceived in multicast services, where common symbols are shared in a multicast group of the vehicles running at different speeds, for reducing the pilot overhead.

2) *Approach*: Our dynamic pilot pattern for doubly selective channel estimation is optimised based on the various speeds of the vehicles within the multicast group, where the length of a multicast block is determined by the channel coherence time of the slowest vehicle in the multicast group. As such,

the pilot overhead is minimised and the effective throughput is improved.

3) *Evaluation*: To verify the validity of our dynamic pilot design in the IoV multicast, its performance over doubly selective channels is formulated and investigated within MIMO-OFDM systems in terms of spectral efficiency and energy efficiency.

D. Structure and Notation

In detailing the above contributions, the remainder of this work is organized as follows. Section II introduces the basics of channel estimation in MIMO systems and the point design for point-to-point doubly selective channels as preliminaries. Section III proposes our dynamic pilot design for doubly selective channel estimation in a multicast service to the vehicles running at different speeds. In contrast to the conventional design of pilot patterns, Section IV evaluates the performance of our dynamic pilot design in terms of overhead rate, spectral efficiency and energy efficiency. Section V concludes the paper.

Throughout this paper, the following mathematical notations are used: Boldface uppercase and lowercase letters denote matrices and vectors, respectively. In particular, $\mathbf{0}_{1 \times M}$ denotes the $1 \times M$ zero vector and \mathbf{I}_M denotes the $M \times M$ identity matrix. Moreover, $\mathcal{E}\{\cdot\}$ represents the expectation (mean) operator, and $\det(\cdot)$ returns the determinant of a square matrix. The transpose, the conjugate transpose, and the modulus operators are denoted by $(\cdot)^T$, $(\cdot)^\dagger$, and $|\cdot|$, respectively. The complex normal distribution with mean μ and variance σ^2 is denoted by $\mathcal{CN}(\mu, \sigma^2)$. The greatest integer function is denoted by $\lfloor \cdot \rfloor$.

In addition, the communication resource units used in this paper are specified in Table II.

II. PRELIMINARIES

A. Channel Estimation in MIMO Systems

In wireless communications, the PSAM is used for the estimation of CSI and, thus, understand the propagation property of a link. Consider an (M, N) flat-fading MIMO channel with M transmit antennas (TAs) and N receive antennas (RAs), as shown in Fig. 1. The $N \times M$ random matrix $\mathbf{H} = [h_{nm}] = [\mathbf{h}_1, \mathbf{h}_2, \dots, \mathbf{h}_M]$ represents the channel matrix in a channel realisation, where the $N \times 1$ vector $\mathbf{h}_m = [h_{1m}, h_{2m}, \dots, h_{Nm}]^T$ contains the flat-fading channel coefficients from TA m to all the N RAs. Herein, all the components in \mathbf{H} are assumed independent and identically distributed (i.i.d.) circularly symmetric complex Gaussian random variables with zero mean and unit variance, i.e., $h_{nm} \sim \mathcal{CN}(0, 1)$, $m = 1, 2, \dots, M$, $n = 1, 2, \dots, N$.

In practice, the block-fading MIMO channel model is adopted for channel estimation, where the i.i.d. channel coefficients in a channel realisation \mathbf{H} are sampled from the complex Gaussian ensemble $\mathcal{CN}(0, 1)$ at the start of each block and remain constant for C symbols. This process is repeated for every block in an i.i.d. manner. Within an arbitrary block, the packet structure of an (M, N) system is illustrated in Fig. 1, where a single pilot symbol b , known at the receiver, is inserted in the packet to be transmitted at a TA for the purpose

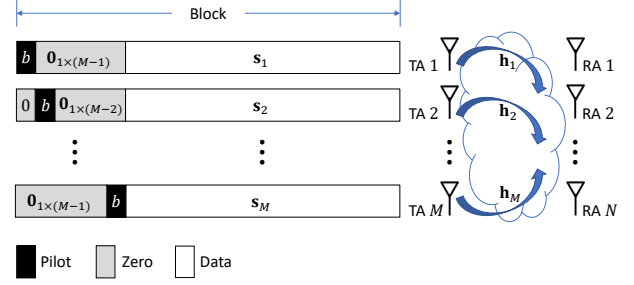


Fig. 1. The packet structure of an (M, N) system within an arbitrary block.

of channel estimation. To avoid the inter-channel interference, the M pilot symbols are evenly interspersed with zeros at the M TAs. More specifically, the zero vectors $\mathbf{0}_{1 \times (m-1)}$ and $\mathbf{0}_{1 \times (M-m)}$ are allocated before and after the pilot symbol at TA $m \in \{1, 2, \dots, M\}$. In this way, the M pilot symbols are alternatively transmitted from all the TAs. Given a block of length C symbols, there are $M - 1$ zeros plus a single pilot symbol used as the overhead for channel estimation at each TA. Thus, the overhead rate is M/C , and the information symbols to be transmitted from TA m are contained by a $1 \times (C - M)$ vector \mathbf{s}_m .

At the receiver, the CSI \mathbf{h}_m , spanning from TA m to all the N RAs, is estimated according to the pilot observations, and then the CSI estimation is used for the coherent detection of the data \mathbf{s}_m , $m = 1, 2, \dots, M$.

The observed pilot symbols originating from TA m is obtained by

$$\mathbf{y}_m = \mathbf{h}_m b + \mathbf{w}_m, \quad (1)$$

where the $N \times 1$ vectors \mathbf{y}_m and \mathbf{w}_m contain the receiver's observations of the pilot symbol originating from TA m and the components of additive white Gaussian noise (AWGN), respectively.

Using the minimum mean square error (MMSE) estimation, the CSI \mathbf{h}_m is estimated by [6], [7]

$$\hat{\mathbf{h}}_m = \frac{b}{|b|^2 + \sigma_W^2} \mathbf{y}_m, \quad (2)$$

where $m = 1, 2, \dots, M$, and σ_W^2 is the AWGN power.

The real CSI \mathbf{h}_m can then be expressed as

$$\mathbf{h}_m = \hat{\mathbf{h}}_m + \tilde{\mathbf{h}}_m, \quad (3)$$

where $\tilde{\mathbf{h}}_m$ contains the channel estimation errors and its variance is $\sigma_{\text{MMSE}}^2 \mathbf{I}_M$. The factor

$$\sigma_{\text{MMSE}}^2 = \frac{1}{1 + |b|^2 / \sigma_W^2} \quad (4)$$

is the MMSE, which is reduced with the increase in the power of a pilot symbol.

B. Pilot Design for Point-to-Point Doubly Selective Channels

The time-frequency selective fading caused by the high mobility of vehicles is a main challenge faced by the IoV. In an (M, N) MIMO system over doubly selective channels, the

TABLE II
DEFINITIONS OF COMMUNICATION RESOURCE UNITS

Unit	Description
Block	The duration of channel coherence time.
Packet	A segment composed of the overhead and data delivered by a single transmit antenna within a block.
Subcarrier	A frequency tone of identical spacing within an OFDM.
Symbol	A digitally modulated signal, e.g., a phase shift keying symbol or a quadrature amplitude modulation symbol.

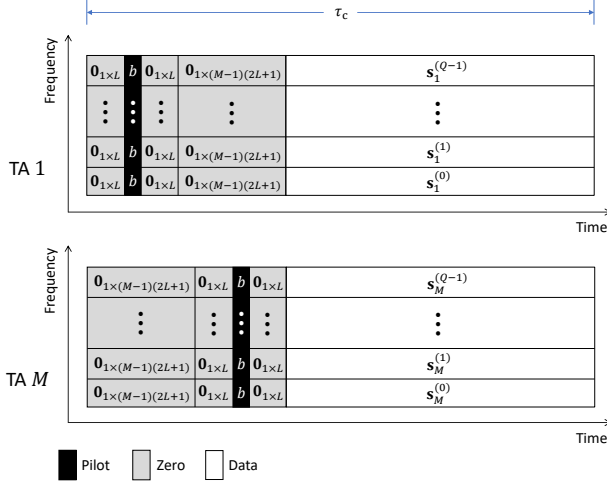


Fig. 2. Pilot design for point-to-point doubly selective channel estimation.

impulse response of the time-varying channel from TA m to RA n is denoted by $h_{nm}(t; \tau)$, where the delay $\tau \in [0, \tau_{\max}]$, with τ_{\max} for the maximum delay spread caused by the multipath, $m = 1, 2, \dots, M$, $n = 1, 2, \dots, N$.

Given the sampling period T_s , the Q subcarriers within an OFDM have equal frequency spacing $\Delta f = (1/T_s)/Q$, and the doubly selective channel estimation needs to capture the variations of Q frequency bases, with $L = \lceil \tau_{\max}/T_s \rceil$ paths in time domain. As such, the impulse response $h_{nm}(t; \tau)$ is expressed as $h_{nm}(k; l)$ in discrete time, where $t = kT_s$ and $\tau = lT_s$, with the discrete-time index $k = 1, 2, \dots$ and the multipath index $l = 0, 1, \dots, L - 1$.

In frequency domain, the transfer function of the channel from TA m to RA n over the q^{th} subcarrier, at the discrete time k , is obtained by

$$H_{nm}(k; q) = \sum_{l=0}^{L-1} h_{nm}(k; l) \exp(-j2\pi lq/Q), \quad (5)$$

$$q = 0, 1, \dots, Q - 1, \quad k = 1, 2, \dots$$

Without loss of generality, the discrete-time index k is omitted hereafter for the sake of simplicity.

If the transmitter is fixed and the receiver is a vehicle running at speed v , the Doppler spread is

$$f_D = v f_c / c, \quad (6)$$

where f_c is the central frequency of the carrier and the constant $c = 3 \times 10^8$ m/s is the speed of light. Thus, the channel

coherence time is given by

$$\tau_c = 1/f_D = c/(v f_c), \quad (7)$$

which is a monotonically decreasing function of v .

The packet structure for the doubly selective channel estimation in a point-to-point MIMO system having M TAs is illustrated in Fig. 2. At each TA, a symbol column in the packet consists of Q subcarriers and these Q symbols are converted into an OFDM waveform in time domain through Q -point inverse fast Fourier transform (IFFT).

The block length is equal to the channel coherence time τ_c . The estimation of the CSI at each subcarrier, $q \in \{0, 1, \dots, Q - 1\}$, from a TA, $m \in \{1, 2, \dots, M\}$, to the receiver relies on a single pilot symbol b , which is surrounded by two $1 \times L$ zero vectors to protect the transmission against multipath propagation. The L zeros before the pilot symbol are used to avoid the inter-symbol interference (ISI) to it, and those after it are used to avoid the ISI from it. Furthermore, to avoid the inter-channel interference among the M TAs, the zero vectors $\mathbf{0}_{1 \times (m-1)(2L+1)}$ and $\mathbf{0}_{1 \times (M-m)(2L+1)}$ are allocated before and after the symbols $[\mathbf{0}_{1 \times L}, b, \mathbf{0}_{1 \times L}]$ at TA $m \in \{1, 2, \dots, M\}$. Following the overhead is the data vector $\mathbf{s}_m^{(q)}$, which contains the data to be transmitted over the q^{th} subcarrier at TA m , $q \in \{0, 1, \dots, Q - 1\}$, $m \in \{1, 2, \dots, M\}$.

For the transmission of unknown information symbols, the cyclic prefix (CP) or zero padding (ZP) is used as a guard interval to protect the OFDM waveforms from the ISI. Since our work is focused on the channel estimation while the CP or ZP is not used for this purpose, the CP or ZP is regarded as a part in the data vectors $\mathbf{s}_m^{(q)}$, $q = 0, 1, \dots, Q - 1$, $m = 1, 2, \dots, M$. As such, there are $M(2L+1)$ symbols used as the overhead, composed of a single pilot symbol and $M(2L+1) - 1$ zeros, for the channel estimation over a subcarrier at each TA within a block. Given a block of length $\lceil \tau_c/T_s \rceil$ symbols, the overhead rate is $M(2L+1)/\lceil \tau_c/T_s \rceil$ for the point-to-point doubly selective channel estimation, and there are $\lceil \tau_c/T_s \rceil - M(2L+1)$ information symbols in each data vector $\mathbf{s}_m^{(q)}$, $q \in \{0, 1, \dots, Q - 1\}$, $m \in \{1, 2, \dots, M\}$.

Within an arbitrary block, the channel transfer function from TA m to RA n over the q^{th} subcarrier, $H_{nm}(q)$, remains constant. To estimate the CSI $H_{nm}(q)$, the observation of a pilot symbol b is expressed as

$$Y_{nm}(q) = H_{nm}(q)b + W_{nm}(q), \quad (8)$$

$$q = 0, 1, \dots, Q - 1,$$

where $Y_{nm}(q)$ is the pilot symbol received by RA n from TA m over the q^{th} subcarrier, and $W_{nm}(q)$ is the accompanying AWGN, $m = 1, 2, \dots, M$, $n = 1, 2, \dots, N$.

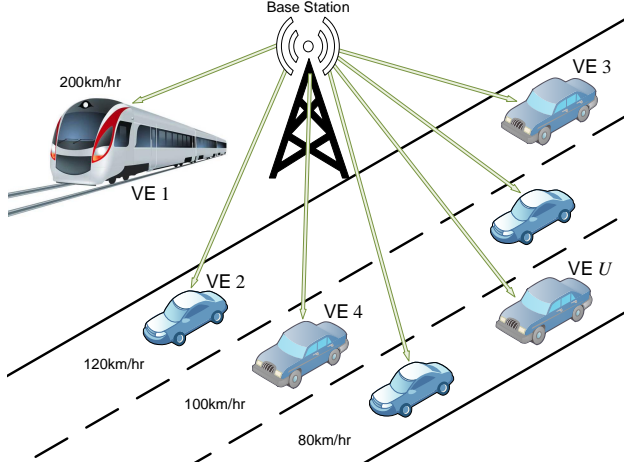


Fig. 3. The IoV multicast to vehicles running at different speeds.

Using the MMSE estimation, the estimated channel transfer function in frequency domain is obtained by

$$\hat{H}_{nm}(q) = \frac{Y_{nm}(q)b}{|b|^2 + \sigma_W^2}, \quad (9)$$

for the coherent detection of the data transmitted in the MIMO-OFDM system. The MMSE in the channel estimation is given by (4).

III. DYNAMIC PILOT DESIGN

Consider the multicast service shown in Fig. 3, where U vehicles (VEs) in the IoV are running at different speeds and they are ordered according to their speeds, i.e., VE 1, VE 2, \dots , VE U pertain to $v_1 \geq v_2 \geq \dots \geq v_U$, where v_u is the speed of VE u , $u = 1, 2, \dots, U$. There are M TAs at the base station. The doubly selective channel estimation at each vehicle needs to capture the variations of Q frequency bases in the OFDM and L paths in the time domain.

As shown in (7), the length of a block in the multicast service is determined by the Doppler spread caused by the vehicles' mobilities. The Doppler spread of the u^{th} vehicle's channel, denoted by f_u , is calculated using

$$f_u = v_u f_c / c, \quad (10)$$

where f_c is the central frequency of the carrier used in the multicast, and $u = 1, 2, \dots, U$.

Obviously, the coherence times of all the U vehicles' channels in the multicast are ordered as $\tau_1 \leq \tau_2 \leq \dots \leq \tau_U$, where $\tau_u = 1/f_u$ is the channel coherence time of VE u and it decreases as the vehicle's speed v_u increases, $u = 1, 2, \dots, U$.

A straightforward way to design the pilot structure for a multicast to these vehicles is individually allocating pilot symbols to each of them based on the coherence time of each point-to-point channel. More specifically, each vehicle's segment is structured in the same way as the block presented in Fig. 2, and a multicast block is an aggregation of all the vehicles' segments. In this way, the overhead rate, i.e., the

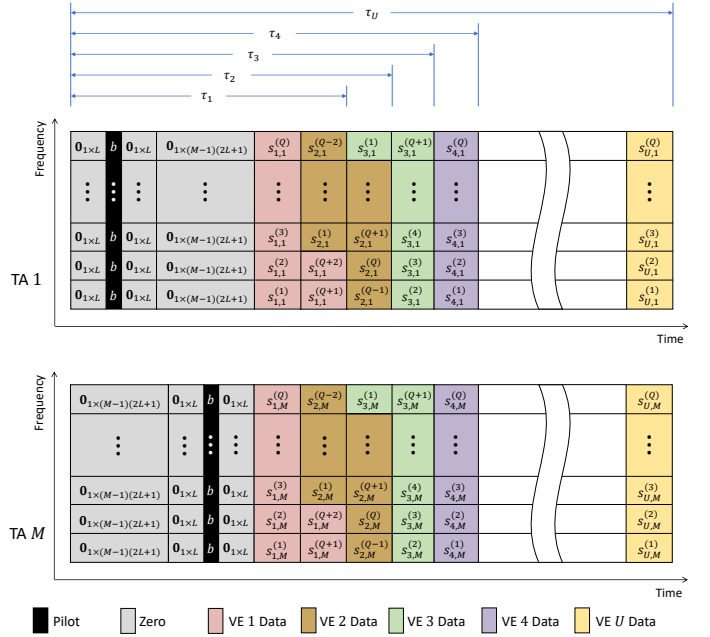


Fig. 4. Dynamic pilot design for the multicast to vehicles running at different speeds.

percentage of pilot symbols plus zeros in a given multicast service, for the doubly selective channel estimation is

$$\lambda_{\text{con}} = \frac{UM(2L+1)}{\sum_{u=1}^U \lfloor \tau_u / T_s \rfloor}, \quad (11)$$

where λ_{con} denotes the overhead rate in the conventional pilot design for the IoV multicast services with MIMO-OFDM transmissions over doubly selective channels.

To reduce the overhead, we propose a dynamic pilot design in the IoV multicast, where common pilot symbols are shared among the U vehicles and the length of a multicast block is set to τ_U , i.e., the longest coherence time among all the vehicles' in multicast group. In this way, the overhead rate for the doubly selective channel estimation is

$$\lambda_{\text{dyn}} = \frac{M(2L+1)}{\lfloor \tau_U / T_s \rfloor}, \quad (12)$$

where λ_{dyn} denotes the overhead rate in our dynamic pilot design for the IoV multicast services with MIMO-OFDM transmissions over doubly selective channels.

Using our dynamic pilot design for the doubly selective channel estimation, the packet structure of a multicast block transmitted from the base station is shown in Fig. 4, where Q subcarriers are available. The multicast block length is equal to the channel coherence time of VE U , i.e., $\lfloor \tau_U / T_s \rfloor$. At TA m , the common overhead $[\mathbf{0}_{1 \times (m-1)(2L+1)}, \mathbf{0}_{1 \times L}, b, \mathbf{0}_{1 \times L}, \mathbf{0}_{1 \times (M-m)(2L+1)}]$ is shared among the U vehicles for the channel estimation over each subcarrier. Afterwards, the data destined for the U vehicles are loaded into the packet at a TA in sequence. The information symbols addressed to the fastest vehicle, i.e., running at speed v_1 , are located closest to the pilot symbols, i.e., within the shortest coherence time τ_1 . Subsequently, the information

symbols addressed to VE u , whose speed is v_u , are located within the coherence time τ_u , $u = 2, \dots, U - 1$. Finally, the information symbols addressed to the slowest vehicle, i.e., at speed v_U , are located at the end of the packet.

The information symbols destined for each vehicle are evenly divided into M segments, and each segment is loaded into the packet at a TA. The segment length of VE u is denoted by P_u . For example, $P_1 = Q + 2$, $P_2 = 2Q - 3$, $P_3 = Q + 1$, $P_4 = Q$ and $P_U = Q$ in Fig. 4. The p^{th} information symbol in the segment of VE u at TA m is denoted by $s_{u,m}^{(p)}$, $m = 1, 2, \dots, M$, $u = 1, 2, \dots, U$, $p = 1, 2, \dots, P_u$.

As such, our dynamic pilot design guarantees that the channel coefficients of every vehicle remain constant from the beginning of the block to the end of the vehicle's information symbols, which allows every vehicle to utilise the common pilot symbols for the doubly selective channel estimation and apply the estimated CSI in its own coherent signal detection.

Given an arbitrary multicast block as shown in Fig. 4, to estimate the channel transfer function from TA m of the base station to RA n at VE u over the q^{th} subcarrier, denoted by $H_{nm}^{(u)}(q)$, the received pilot symbol in frequency domain is expressed as

$$Y_{nm}^{(u)}(q) = H_{nm}^{(u)}(q)b + W_{nm}^{(u)}(q), \quad (13)$$

$$m = 1, 2, \dots, M, \quad n = 1, 2, \dots, N_u,$$

where $Y_{nm}^{(u)}(q)$ and $W_{nm}^{(u)}(q)$ are the observed pilot symbol and the received AWGN, respectively, over the q^{th} subcarrier from TA m of the base station to RA n at VE u , $q = 0, 1, \dots, Q - 1$, $u = 1, 2, \dots, U$. The number of RAs at VE u is denoted by N_u .

Using the MMSE estimation, the estimated CSI from TA m to RA n over the q^{th} subcarrier at VE u is obtained by

$$\hat{H}_{nm}^{(u)}(q) = \frac{Y_{nm}^{(u)}(q)b}{|b|^2 + \sigma_W^2}, \quad (14)$$

and the MMSE is given by (4).

IV. PERFORMANCE EVALUATION

To evaluate the performance and resource utilisation of our dynamic pilot design, the overhead rate, spectral efficiency and energy efficiency are formulated as the metrics to investigate its overhead reduction, achievable data rate and effective energy consumption, respectively.

A. Packet Structure

The packet structure with our dynamic pilot design is shown in Fig. 4, which is determined by the range of the vehicles' speeds, i.e., $[v_U, v_1]$. In practice, all the vehicles running over a section or a lane of the highway maintain almost the same speed, as illustrated in Fig. 3. If there are a huge number of vehicles in the IoV multicast group, the range of their speeds is partitioned into U non-overlapping consecutive intervals $[v_u, v_{u-1}]$, $U = 1, 2, \dots, U$, where v_0 is an arbitrarily small increment above the highest speed v_1 for the practical purpose of QoS guarantee. Thus, the vehicles are divided into subgroups according to their speeds. More

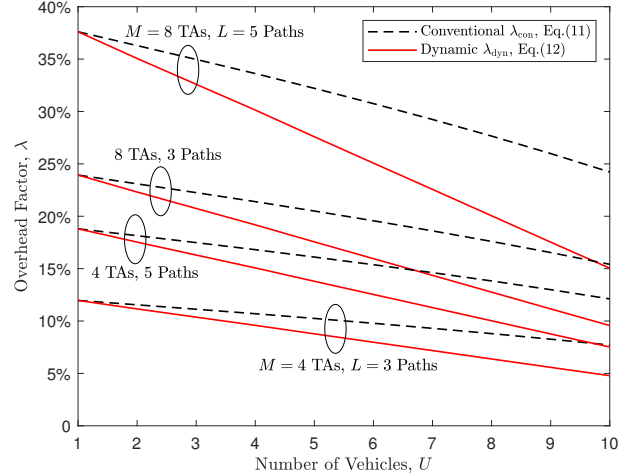


Fig. 5. Overhead rates λ_{con} in (11) and λ_{dyn} in (12) versus the number of vehicles, U , with the highest speed $v_1 = 150$ km/hr.

specifically, the information symbols addressed to the vehicles running at any speed in $[v_u, v_{u-1}]$ are located within the time slot $(\tau_{u-1}, \tau_u]$, where τ_0 is the start of the multicast data, i.e., the end of the pilot overhead.

For the sake of simplicity, it is assumed that each subgroup contains a single vehicle in the performance evaluation. Since the packet structure is specified by the various speeds the vehicles are running at, which is unrelated to the number of vehicles in each subgroup, the performance and resource utilisation efficiency remain the same no matter how many vehicles are destined for each subgroup, as long as the information symbols addressed to them can be accommodated into the specified time slot.

In particular, the comparisons between our dynamic pilot design and conventional pilot design are investigated in the IoV multicast with MIMO-OFDM transmissions over doubly selective channels for U vehicles running at different speeds. The central frequency of the carrier used in the multicast is $f_c = 2.4$ GHz [36], and the sampling period is set to $T_s = 12.8 \mu\text{s}$ [37]. The various speeds of the U vehicles are set to $v_u = v_1 - 10(u - 1)$ km/hr, $u = 1, 2, \dots, U$, where v_1 is the highest speed and v_U is the slowest speed among the U vehicles'. For example, if there are $U = 5$ vehicles in the IoV multicast and VE 1 is running at $v_1 = 150$ km/hr, the other vehicles are running at $v_2 = 140$ km/hr, $v_3 = 130$ km/hr, $v_4 = 120$ km/hr, and $v_5 = 110$ km/hr, respectively.

B. Overhead Rate

The overhead rate is a metric to measure how much communication resource is dedicated to the channel estimation, for delivering a certain amount of multicast data. This metric is defined as the ratio of the dedicated resource for channel estimation to the total resource consumed in a multicast block.

To begin with, the overhead rate of our dynamic pilot design, λ_{dyn} given by (12), and that of the conventional pilot design, λ_{con} given by (11), are compared in Fig. 5, where both overhead rates are plotted versus the number of vehicles,

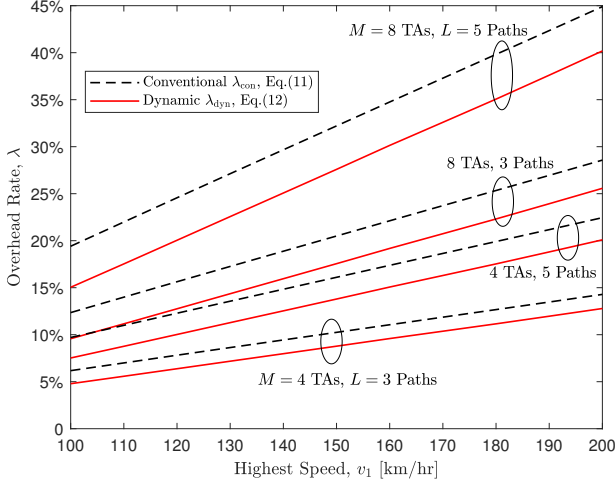


Fig. 6. Overhead rates λ_{con} in (11) and λ_{dyn} in (12) versus the highest speed v_1 among the $U = 5$ vehicles in the multicast services.

U , in the IoV multicast. Herein, the highest speed among the U vehicles' is set to $v_1 = 150$ km/hr. As shown in this figure, both λ_{dyn} and λ_{con} get higher with the increase in the number of time-domain paths, L , or the number of TAs, M . On the other hand, λ_{dyn} and λ_{con} get lower with the increase in the number of vehicles, U . If there is a single vehicle only, i.e., $U = 1$, the overhead rate of our dynamic pilot design is the same as that of conventional pilot design, which can be observed by comparing (12) and (11) as well. More specifically, given that $U = 1$, we have

$$\lambda_{\text{dyn}} = \lambda_{\text{con}} = \frac{M(2L+1)}{[\tau_1/T_s]}. \quad (15)$$

As the number of vehicles, U , increases, the gap between λ_{con} and λ_{dyn} gets larger. In other words, our dynamic pilot design saves more overhead, i.e., more pilot symbols and zeros, compared with the conventional pilot design, given more vehicles in the IoV.

In Fig. 6, the overhead rates λ_{dyn} and λ_{con} are plotted versus the highest speed $v_1 \in [100, 200]$ km/hr in the multicast services, where $U = 5$ vehicles are in the IoV. As shown in this figure, both λ_{dyn} and λ_{con} get higher as v_1 increases, which implies that more overhead is needed as the speeds increase for both the conventional pilot design and the dynamic pilot design. However, the difference $\lambda_{\text{con}} - \lambda_{\text{dyn}}$ remains almost the same with the increase in v_1 . Elaborating a bit further, the overhead rate difference $\lambda_{\text{con}} - \lambda_{\text{dyn}}$ versus the highest speed v_1 is depicted in Fig. 7. As shown in this figure, more overhead is saved by our dynamic pilot design in comparison to the conventional pilot design, as the number of time-domain paths, L , or the number of TAs, M , increases.

C. Spectral Efficiency

The spectral efficiency is a metric to measure how efficiently a certain amount of communication resource is utilised in the multicast, taking into account the overhead for channel estimation and the accuracy of channel estimation. This metric

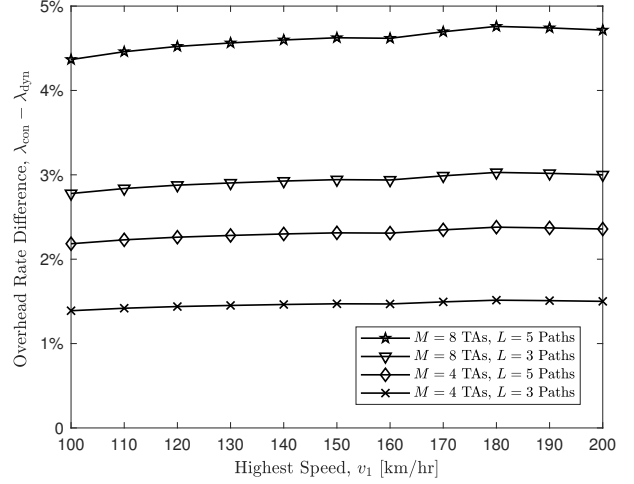


Fig. 7. Overhead difference between our dynamic pilot design and the conventional pilot design, $\lambda_{\text{con}} - \lambda_{\text{dyn}}$, versus the highest speed v_1 among the $U = 5$ vehicles in the multicast services.

is defined as the effective data rate that can be achieved by a specific communication system using the given resource.

Based on the concept of physical-layer channel capacity [38], [39], the achievable data rate of the IoV multicast services in MIMO-OFDM systems with channel estimation can be calculated using

$$R = \mathcal{E} \left\{ \frac{1}{U} \sum_{u=1}^U \log_2 \det \left(\mathbf{I}_N + \frac{\rho(1 - \sigma_{\text{MMSE}}^2)}{1 + \rho\sigma_{\text{MMSE}}^2} \hat{\mathbf{H}}_u \hat{\mathbf{H}}_u^\dagger \right) \right\} \quad (16)$$

in the unit of [bits/sec/Hz], where U is the number of vehicles in the IoV, and σ_{MMSE}^2 is given by (4). Without loss of generality, over an arbitrary subcarrier, at the given signal-to-noise power ratio (SNR) ρ , the estimated CSI of the u^{th} vehicle's (M, N) flat-fading MIMO channel is modelled as [40], [41]

$$\hat{\mathbf{H}}_u = \mathbf{H}_u + \sigma_{\hat{H}} \mathbf{\Omega}, \quad (17)$$

where the $N \times M$ matrix $\hat{\mathbf{H}}_u$ contains the estimated CSI, and the $N \times M$ matrix \mathbf{H}_u is the real channel matrix of VE $u \in \{1, 2, \dots, U\}$. The i.i.d. entries of the $N \times M$ matrix $\mathbf{\Omega}$ have the distribution $\mathcal{CN}(0, 1)$. Further, the CSI estimation accuracy is measured by $\sigma_{\hat{H}} = \sqrt{\sigma_{\text{MMSE}}^2}$. More specifically, the CSI estimation accuracy using our dynamic pilot design, with much lower overhead, is the same as that of the conventional pilot design.

Concerning the overhead for channel estimation, the spectral efficiency of the IoV multicast using our dynamic pilot design is defined as

$$\eta_{\text{dyn}} = (1 - \lambda_{\text{dyn}})R, \quad (18)$$

where λ_{dyn} is given by (12) and R is given by (16).

Similarly, the spectral efficiency of the IoV multicast using the conventional pilot design is obtained by

$$\eta_{\text{con}} = (1 - \lambda_{\text{con}})R, \quad (19)$$

where λ_{con} is given by (11).

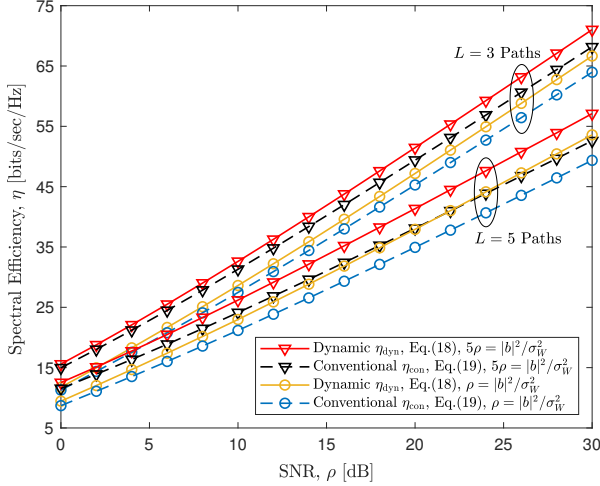
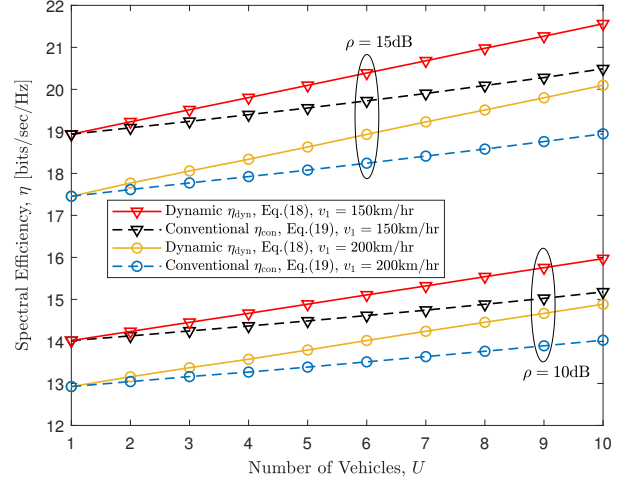


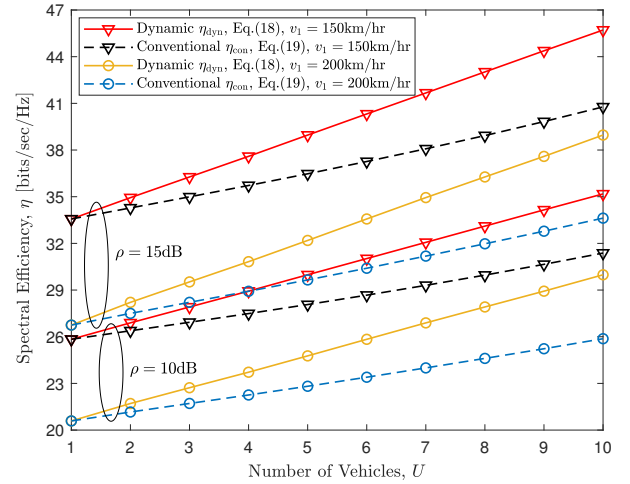
Fig. 8. Spectral efficiency comparisons between our dynamic pilot design and conventional pilot design, in the IoV multicast services for $U = 5$ vehicles, with the highest speed among the vehicles' $v_1 = 200$ km/hr and the antenna configuration $M = N = 8$.

Fig. 8 compares the spectral efficiency of our dynamic pilot design, η_{dyn} achieved by (18), against that of the conventional pilot design, η_{con} achieved by (19), in the IoV multicast services for $U = 5$ vehicles, with $M = 8$ TAs at the base station and $N = 8$ RAs at each vehicle. The highest speed among the five vehicles' is $v_1 = 200$ km/hr. Herein, two power allocation schemes are utilised: (i) the transmit power of a pilot symbol is the same as that of a single information symbol, i.e., the SNR $\rho = |b|^2/\sigma_W^2$, and the MMSE of the channel estimation $\sigma_{\text{MMSE}}^2 = 1/(1 + \rho)$; (ii) the transmit power of a pilot symbol is five times that of a single information symbol, i.e., $5\rho = |b|^2/\sigma_W^2$, and $\sigma_{\text{MMSE}}^2 = 1/(1 + 5\rho)$. The number of time-domain paths for each vehicle's channel is set to $L = 3$ and 5. As shown in this figure, both η_{dyn} and η_{con} get higher with the increase in the SNR. Moreover, both our dynamic pilot design and the conventional counterpart achieve higher spectral efficiency in the case of $5\rho = |b|^2/\sigma_W^2$. Elaborating slightly further, higher transmit power allocated to the pilot symbols yields smaller MMSE, i.e., higher accuracy of the CSI estimation, which therefore leads to higher spectral efficiency. In addition, our dynamic pilot design achieves higher spectral efficiency than the conventional counterpart. The gap between η_{dyn} and η_{con} is increased as the number of time-domain paths, L , increases. The main reason behind this is that the spectral efficiency difference between our dynamic pilot design and the conventional counterpart is determined by the overhead rate difference between them, i.e., $\lambda_{\text{con}} - \lambda_{\text{dyn}}$, which gets larger with the growth of L as shown in Fig. 7.

In Fig. 9, the spectral efficiencies η_{dyn} and η_{con} are plotted versus the number of vehicles, U , for two antenna configurations, i.e., $M = N = 4$ and $M = N = 8$, where the highest speed among the U vehicles' is set to $v_1 = 150$ km/hr and 200 km/hr. The number of time-domain paths for each vehicle's channel is $L = 5$, and the transmit power of a pilot symbol is twice that of a single information symbol, i.e., $2\rho = |b|^2/\sigma_W^2$, and the MMSE of the channel estimation



(a) $M = N = 4$



(b) $M = N = 8$

Fig. 9. Spectral efficiency versus the number of vehicles, U , with $L = 5$ time-domain paths over each vehicle's channel, given the power allocation $2\rho = |b|^2/\sigma_W^2$.

$\sigma_{\text{MMSE}}^2 = 1/(1 + 2\rho)$. As shown in this figure, both η_{dyn} and η_{con} get higher with the increase in the number of vehicles, U . The main reason behind this is that both overhead rates λ_{dyn} and λ_{con} are reduced as U increases, which has been shown in Fig. 5. Moreover, the gap between η_{dyn} and η_{con} gets larger as U increases, since the difference $\lambda_{\text{con}} - \lambda_{\text{dyn}}$ gets larger as U increases. Further, both η_{dyn} and η_{con} are improved as the highest speed among all vehicles, v_1 , decreases. This is because both overhead rates λ_{dyn} and λ_{con} are reduced as v_1 decreases, which has been shown in Fig. 6. Besides, comparing Fig. 9(a) with Fig. 9(b), we may find that both η_{dyn} and η_{con} are improved dramatically given more TAs at the base station and/or more RAs at each vehicle.

D. Energy Efficiency

The energy efficiency is a metric to measure how much information can be transmitted given a certain power consumption, based on which the power needed to transmit a certain

amount of information can be obtained in a straightforward way. This metric is defined as the number of information bits over a unit of power consumption.

More specifically, the energy efficiency of a communication system is expressed in the unit of [bits/joule] as [42]

$$\zeta = R_e/P_T, \quad (20)$$

where R_e is the effective transmission rate in the unit of [bits/sec], and P_T is the total transmit power in the unit of [joules/sec].

Using our dynamic pilot design, the energy efficiency of the IoV multicast services in MIMO-OFDM transmissions is obtained by

$$\begin{aligned} \zeta_{\text{dyn}} &= \frac{Q\eta_{\text{dyn}}}{Q|b|^2 + Q\lfloor\tau_U/T_s\rfloor P_s - QM(2L+1)P_s} \\ &= \frac{(1-\lambda_{\text{dyn}})R}{|b|^2 + \lfloor\tau_U/T_s\rfloor P_s - M(2L+1)P_s}, \end{aligned} \quad (21)$$

where Q is the number of subcarriers available in the IoV multicast, and $Q\eta_{\text{dyn}}$ is the effective transmission rate using our dynamic pilot design, with η_{dyn} given in (18). The total transmit power of pilot symbols is $Q|b|^2$ and the total transmit power of information symbols is $Q\lfloor\tau_U/T_s\rfloor P_s - QM(2L+1)P_s$, with P_s denoting the transmit power of a single information symbol.

Using the conventional pilot design, the energy efficiency of the IoV multicast services in MIMO-OFDM transmissions is expressed as

$$\begin{aligned} \zeta_{\text{con}} &= \frac{Q\eta_{\text{con}}}{Q|b|^2 + QP_s \sum_{u=1}^U \lfloor\tau_u/T_s\rfloor - QP_s UM(2L+1)} \\ &= \frac{(1-\lambda_{\text{con}})R}{|b|^2 + P_s \sum_{u=1}^U \lfloor\tau_u/T_s\rfloor - P_s UM(2L+1)}, \end{aligned} \quad (22)$$

where $Q\eta_{\text{con}}$ is the effective transmission rate using the conventional pilot design, with η_{con} given in (19), and the total transmit power of unknown information symbols is $QP_s \sum_{u=1}^U \lfloor\tau_u/T_s\rfloor - QP_s UM(2L+1)$.

Fig. 10 compares the energy efficiency of our dynamic pilot design, ζ_{dyn} achieved by (21), against that of the conventional pilot design, ζ_{con} achieved by (22), in the IoV multicast services for $U = 5$ vehicles, with $M = 8$ TAs at the base station and $N = 8$ RAs at each vehicle. The highest speed among the five vehicles' is $v_1 = 200$ km/hr. Herein, two power allocation schemes are utilised: (i) the transmit power of a pilot symbol is the same as that of a single information symbol, i.e., $|b|^2 = P_s$, and (ii) the transmit power of a pilot symbol is five times that of a single information symbol, i.e., $|b|^2 = 5P_s$. The number of time-domain paths for each vehicle's channel is set to $L = 3$ and 10. As shown in this figure, the change in the number of time-domain paths, L , has slight influence on the energy efficiency, mainly because L determines the length of zero vectors which, however, does not consume transmit power. Both ζ_{dyn} and ζ_{con} get higher as the SNR $\rho = P_s/\sigma_W^2$ increases. Moreover, the gap between ζ_{dyn} and ζ_{con} is increased as the SNR increases. Furthermore, both our dynamic pilot design and the conventional counterpart achieve higher energy efficiency in the case of $|b|^2 = 5P_s$. In other

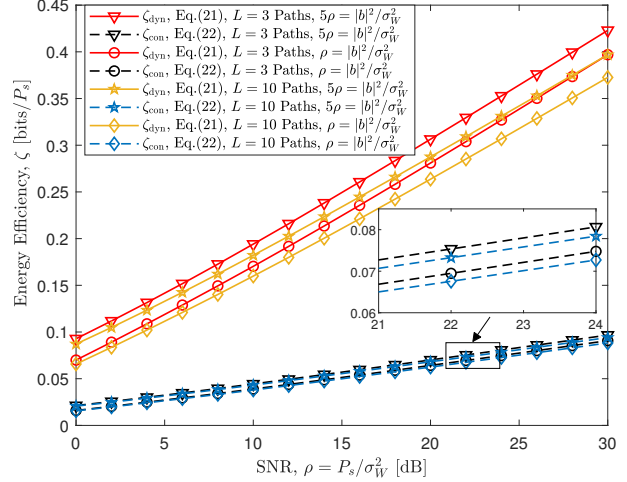


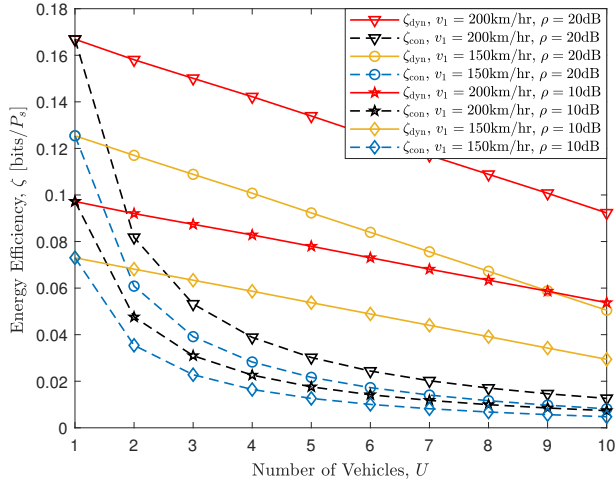
Fig. 10. Energy efficiency comparisons between our dynamic pilot design and conventional pilot design, in the IoV multicast services for $U = 5$ vehicles, with the highest speed among the vehicles' $v_1 = 200$ km/hr and the antenna configuration $M = N = 8$.

words, the contribution of higher CSI estimation accuracy to the throughput exceeds the impact of higher pilot power consumption.

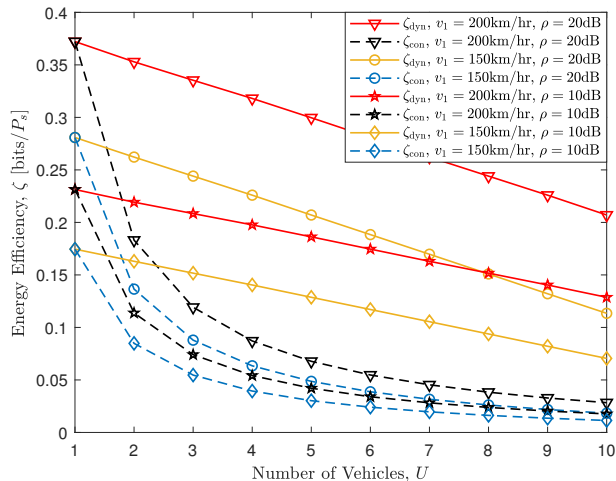
In Fig. 11, the energy efficiencies ζ_{dyn} and ζ_{con} are plotted versus the number of vehicles, U , for two antenna configurations, i.e., $M = N = 4$ and $M = N = 8$, where the highest speed among the U vehicles' is set to $v_1 = 150$ km/hr and 200 km/hr. The number of time-domain paths in each vehicle's channel is $L = 5$, and the transmit power of a pilot symbol is twice that of a single information symbol, i.e., $|b|^2 = 2P_s$. As shown in this figure, both ζ_{dyn} and ζ_{con} get lower with the increase in the number of vehicles, U . The main reason behind this is that the throughput gain cannot compensate the loss of pilot power consumption as U increases. Moreover, the gap between η_{dyn} and η_{con} gets smaller as U increases, mainly because the impact of pilot power consumption on both energy efficiencies gets stronger with the increase in U . Different from the increment in the spectral efficiencies η_{dyn} and η_{con} , both energy efficiencies ζ_{dyn} and ζ_{con} are reduced as the highest speed among all vehicles, v_1 , decreases, which is also because the throughput gain cannot compensate the loss of pilot power consumption.

V. CONCLUSION

In this paper, a novel transmission strategy, based on dynamic pilot design, was proposed to reduce the pilot consumption and, therefore, improve the resource utilisation efficiency for doubly selective channel estimation in the IoV multicast services with MIMO-OFDM transmissions, where the vehicles are running at different speeds. Using our dynamic pilot design, a multicast block was defined as the coherence time of the slowest vehicle in the multicast group, and common pilot symbols have been shared among all the vehicles in this multicast block. The multicast information symbols for different vehicles were loaded into the block according to their own coherence times.



(a) $M = N = 4$



(b) $M = N = 8$

Fig. 11. Energy efficiency versus the number of vehicles, U , with $L = 5$ time-domain paths over each vehicle's channel, given the power allocation $|b|^2 = 2P_s$.

To evaluate the performance and resource utilisation of our dynamic pilot design, the metrics of overhead rate, spectral efficiency, and energy efficiency have been formulated, based on which our dynamic pilot design was compared with the conventional counterpart. The comparisons substantiated that our dynamic pilot design outperforms the conventional pilot design. In addition, several important insights have been reached for the pilot design in the IoV multicast services with MIMO-OFDM transmissions over doubly selective channels. Specifically, the overhead rate is reduced as the number of vehicles increases or as the highest speed among the vehicles' decreases. Meanwhile, the spectral efficiency is improved, whilst the energy efficiency gets lower.

As shown in Figs. 1, 2, and 4, the pilot symbols pertaining to all the M TAs are evenly interspersed with zeros to guarantee there is no inter-channel interference at all in the channel estimation process. However, the inter-channel interference is a significant challenge in the data transmission process,

especially using the spatial multiplexing techniques. Further improvement of the data transmission performance in practical MIMO-OFDM systems over doubly selective channels is to be pursued in future research, by exploiting the dynamic pilot design in channel estimation.

ACKNOWLEDGEMENT

The authors would like to thank the editor and the anonymous reviewers for their valuable comments to improve the presentation of this paper.

REFERENCES

- [1] K. Liu, *et al.*, "A Hierarchical Architecture for the Future Internet of Vehicles", *IEEE Commun. Mag.*, vol. 57, no. 7, pp. 41-47, Jul. 2019.
- [2] M. Giordani, *et al.*, "Toward 6G Networks: Use Cases and Technologies", *IEEE Commun. Mag.*, vol. 58, no. 3, pp. 55-61, Mar. 2020.
- [3] D. Wang, *et al.*, "Resource Allocation and Performance Analysis for Multiuser Video Transmission over Doubly Selective Channels", *IEEE Trans. Wireless Commun.*, vol. 14, no. 4, pp. 1954-1966, Apr. 2015.
- [4] W. Chin, "Nondata-Aided Doppler Frequency Estimation for OFDM Systems Over Doubly Selective Fading Channels", *IEEE Trans. Commun.*, vol. 66, no. 9, pp. 4211-4221, Sep. 2018.
- [5] J. K. Cavers, "An analysis of pilot symbol assisted modulation for Rayleigh fading channels", *IEEE Trans. Veh. Technol.*, vol. 40, pp. 86-693, Nov. 1991.
- [6] Y. Yang, N. Bonello, and S. Aissa, "An information-guided channel-hopping scheme for block-fading channels with estimation errors", in *Proc. IEEE Global Commun. Conf. (GLOBECOM)*, Miami, Dec. 2010, pp. 1-5.
- [7] Y. Yang and S. Aissa, "Information-guided communications in MIMO systems with channel state impairments", *Wirel. Commun. Mob. Comput.*, vol. 15, pp. 868-878, 2015.
- [8] X. Ma, G. Giannakis, and S. Ohno, "Optimal training for block transmissions over doubly selective wireless fading channels", *IEEE Trans. Signal Process.*, vol. 51, no. 5, pp. 1351-1366, May. 2003.
- [9] Y. Yang, M. Ma, and B. Jiao, "A design for increasing spectral efficiency of PSAM-OFDM system based on segmented effective transmission rate", *Acta Electronica Sinica*, vol. 35, no. 9, pp. 1660-1664, Sep. 2007.
- [10] Y. Yang, M. Ma, H. Cheng, B. Jiao and W. C. Y. Lee, "A study on segmented data rates for system capacity", in *Proc. IEEE Veh. Technol. Conf. (VTC)*, Baltimore, Oct. 2007, pp. 1106-1108.
- [11] Y. Yang, M. Ma, B. Jiao, and W. C. Y. Lee, "A Design of Segmented Data Rates for Recurrent Channel Estimation", *Wireless Pers. Commun.*, vol. 50, pp. 483-491, 2009.
- [12] J. Oh, J. Kim, and J. Lim, "On the Design of Pilot Symbols for OFDM Systems over Doubly-Selective Channels", *IEEE Commun. Lett.*, vol. 15, no. 12, pp. 1335-1337, Dec. 2011.
- [13] M. Karami, A. Olfat, and N. Beaulieu, "Pilot Symbol Parameter Optimization Based on Imperfect Channel State Prediction for OFDM Systems", *IEEE Trans. Commun.*, vol. 61, no. 6, pp. 2557-2567, Jun. 2013.
- [14] X. Guo, S. Chen, J. Zhang, X. Mu and L. Hanzo, "Optimal Pilot Design for Pilot Contamination Elimination/Reduction in Large-Scale Multiple-Antenna Aided OFDM Systems", *IEEE Trans. Wireless Commun.*, vol. 15, no. 11, pp. 7229-7243, Nov. 2016.
- [15] N. Aboutorab, W. Hardjawana, and B. Vucetic, "A New Iterative Doppler-Assisted Channel Estimation Joint With Parallel ICI Cancellation for High-Mobility MIMO-OFDM Systems", *IEEE Trans. Veh. Technol.*, vol. 61, no. 4, pp. 1577-1589, May 2012.
- [16] J. Gao and H. Liu, "Low-Complexity Map Channel Estimation for Mobile MIMO-OFDM Systems", *IEEE Trans. Wireless Commun.*, vol. 7, no. 3, pp. 774-780, Mar. 2008.
- [17] Q. Li, *et al.*, "Information-Guided Pilot Insertion for OFDM-Based Vehicular Communications Systems", *IEEE Internet Things J.*, vol. 6, no. 1, pp. 26-37, Feb. 2019.
- [18] Y. Yang, S. Dang, Y. He, and M. Guizani, "Markov Decision-Based Pilot Optimization for 5G V2X Vehicular Communications", *IEEE Internet Things J.*, vol. 6, no. 1, pp. 1090-1103, Feb. 2019.
- [19] Y. Yang, "Permutation-based transmissions in ultra-reliable and low-latency communications", *IEEE Commun. Lett.*, vol. 25, no. 3, pp. 1024-1028, Mar. 2021.

- [20] Y. Yang and L. Hanzo, "Permutation-based TCP and UDP transmissions to improve goodput and latency in the Internet-of-Things", *IEEE Internet Things J.*, vol. 8, no. 18, pp. 14276-14286, Sep. 2021.
- [21] F. Yang, P. Cai, H. Qian and X. Luo, "Pilot Contamination in Massive MIMO Induced by Timing and Frequency Errors", *IEEE Trans. Wireless Commun.*, vol. 17, no. 7, pp. 4477-4492, July 2018.
- [22] B. Gong, L. Gui, Q. Qin, X. Ren and W. Chen, "Block Distributed Compressive Sensing-Based Doubly Selective Channel Estimation and Pilot Design for Large-Scale MIMO Systems", *IEEE Trans. Veh. Technol.*, vol. 66, no. 10, pp. 9149-9161, Oct. 2017.
- [23] S. Srivastava, J. Nath and A. K. Jagannatham, "Data Aided Quasistatic and Doubly-Selective CSI Estimation Using Affine-Precoded Superimposed Pilots in Millimeter Wave MIMO-OFDM Systems", *IEEE Trans. Veh. Technol.*, vol. 70, no. 7, pp. 6983-6998, July 2021.
- [24] C. S. Reddy, P. Priya, D. Sen and C. Singhal, "Spectral Efficient Modem Design with OTFS Modulation for Vehicular-IoT System", *IEEE Internet Things J.*, DoI: 10.1109/IJOT.2022.3211531.
- [25] Ericsson Mobility Report. [Online Available Nov. 2021] <https://www.ericsson.com/4ad7e9/assets/local/reports-papers/mobility-report/documents/2021/ericsson-mobility-report-november-2021.pdf>
- [26] M. Alodeh, *et al.*, "Symbol-Level and Multicast Precoding for Multiuser Multiantenna Downlink: A State-of-the-Art, Classification, and Challenges", *IEEE Commun. Surveys Tuts.*, vol. 20, no. 3, pp. 1733-1757, 3rd Quart. 2018.
- [27] Y. Yang and S. Aissa, "Cross-layer combining of information-guided transmission with network coding relaying for multiuser cognitive radio systems", *IEEE Wireless Commun. Lett.*, vol. 2, no. 1, pp. 26-29, Feb. 2013.
- [28] Y. Yang and S. Aissa, "On the coexistence of primary and secondary users in spectrum-sharing broadcast channels", in *Proc. IEEE Int. Conf. Commun. (ICC)*, Budapest, Jun. 2013, pp. 3085-3089.
- [29] Y. Yang and S. Aissa, "Spectrum-sharing broadcast channels using fountain codes: Energy, delay and throughput", *IET Commun.*, vol. 8, no. 14, pp. 2574-2583, Aug. 2014.
- [30] Y. Yang, K. Salama and S. Aissa, "Interference mitigation for broadcast in hierarchical cell structure networks: Transmission strategy and area spectral efficiency", *IEEE Trans. Veh. Technol.*, vol. 63, no. 8, pp. 3818-3828, Oct. 2014.
- [31] Y. Yang, S. Aissa, A. Eltawil and K. Salama, "An interference cancellation strategy for broadcast in hierarchical cell structure", in *Proc. IEEE Global Commun. Conf. (GLOBECOM)*, Austin, Dec. 2014, pp. 1792-1797.
- [32] Y. Yang, "On the capacity of maximum selection in MIMO multicast network", in *Proc. IEEE INFOCOM Workshops*, Apr. 2008, pp. 1-5.
- [33] Y. Yang and S. Aissa, "Common information multicast with different data rates", in *Proc. IEEE Veh. Technol. Conf. (VTC)*, Taipei, Jun. 2010, pp. 1-5.
- [34] Y. Yang and S. Aissa, "On the capacity of multiple cognitive links through common relay under spectrum-sharing constraints", in *Proc. IEEE Int. Conf. Commun. (ICC)*, Kyoto, Jun. 2011, pp. 1-5.
- [35] T. Tran, *et al.*, "Enabling Multicast and Broadcast in the 5G Core for Converged Fixed and Mobile Networks", *IEEE Trans. Broadcast.*, vol. 66, no. 2, pp. 428-439, Jun. 2020.
- [36] Y. Wang, *et al.*, "WiCop: Engineering WiFi Temporal White-Spaces for Safe Operations of Wireless Personal Area Networks in Medical Applications", *IEEE Trans. Mobile Comput.*, vol. 13, no. 5, pp. 1145-1158, May 2014.
- [37] S. Srivastava, *et al.*, "Sparse Doubly-Selective Channel Estimation Techniques for OSTBC MIMO-OFDM Systems: A Hierarchical Bayesian Kalman Filter Based Approach", *IEEE Trans. Commun.*, vol. 68, no. 8, pp. 4844-4858, Aug. 2020.
- [38] S. Verdu, "Spectral efficiency in the wideband regime", *IEEE Trans. Inf. Theory*, vol. 48, no. 6, pp. 1319-1343, Jun. 2002.
- [39] L. Wei, Y. Yang and B. Jiao, "Secrecy throughput in full-duplex multiuser MIMO short-packet communications", *IEEE Wireless Commun. Lett.*, vol. 10, no. 6, pp. 1339-1343, Jun. 2021.
- [40] M. Yin, Y. Yang and B. Jiao, "Security-oriented trellis code design for spatial modulation", *IEEE Trans. Wireless Commun.*, vol. 20, no. 3, pp. 1875-1888, Mar. 2021.
- [41] Y. Yang and W. Li, "Security-oriented polar coding based on channel-gain-mapped frozen bits", *IEEE Trans. Wireless Commun.*, vol. 21, no. 8, pp. 6584-6596, Aug. 2022.
- [42] E. Bjornson, J. Hoydis, and L. Sanguinetti, *Massive MIMO Networks: Spectral, Energy, and Hardware Efficiency*, now, 2017.



Yuli Yang (Senior Member, IEEE) received the Ph.D. degree in Communications & Information Systems from Peking University, China, in July 2007. Her industry experience includes working with Huawei Technologies as an Intern Researcher from June 2006 to July 2007, and with Bell Labs Shanghai as a Research Scientist from August 2007 to December 2009. From January 2010 to December 2019, she was with King Abdullah University of Science & Technology, Melikşah University, and the University of Chester on various academic positions.

Since December 2019, she has been with the University of Lincoln as a Senior Lecturer in Electrical/Electronic Engineering. Her research interests include modelling, design, analysis and optimization of wireless systems and networks, specifically in physical-layer security, permutation-based modulation/transmission, ultra-reliable and low-latency communications.



Bingli Jiao (Senior Member, IEEE) received the B.S. and M.S. degrees from Peking University, China, in 1983 and 1988, respectively, and the Ph.D. degree from Saarland University, Germany, in 1995. He became an Associate Professor in 1995 and a Professor with Peking University in 2000. He currently is the director of Wireless Communication and Signal Processing Research Center, Peking University, Beijing, China. He is also a director of the Joint Laboratory for Advanced Communication Research between Peking University and Princeton

University. His current research interests include full-duplex communications, information theory, and signal processing. He is a pioneer of co-frequency and co-time full-duplex as found in his early patent in 2006.